Diamond & Related Materials 95 (2019) 60–70

Contents lists available at ScienceDirect

Diamond & Related Materials

journal homepage: www.elsevier.com/locate/diamond

Comparison between corrosion behaviour of DLC and N-DLC coatings deposited by DC-pulsed PACVD technique

Omid Sharifahmadian, Farzad Mahboubi*, Sepehr Yazdani

Department of Mining and Metallurgical Engineering, Amirkabir University of Technology (Tehran Polytechnic), P.O. Box 1875-4413, Tehran, Iran

ARTICLE INFO

Keywords:
PACVD
Corrosion
XPS
Diamond-like carbon
Nitrogen

ABSTRACT

DC-pulsed PACVD technique was employed for deposition of nitrogen-doped DLC and DLC coatings on 316 stainless steel. The Raman spectroscopy and AFM analysis were utilized to evaluate the structural properties and surface morphology of the coatings. In order to investigate the wettability of the samples, surface energy was calculated using optical contact angle. Potentiodynamic polarization and EIS tests were applied to assess the corrosion behaviour of the specimens. Moreover, XPS investigation was undertaken in order to study corrosion mechanism of the coatings after immersion in 3.5 wt% NaCl solution for one week. It was found that the DLC coating has better corrosion resistance compared to N-DLC coating. Furthermore, higher reduction of C—C (sp^2) bonds compared to C—C (sp^3) bonds was observed after the immersion test. Additionally, the amount of C═O and COOH bonds in DLC coatings increased more than N-DLC coating.

1. Introduction

Diamond-Like Carbon (DLC) coating has been of interest to researchers due to its exclusive properties such as excellent wear resistance, biocompatibility, and proper corrosion resistance [1–3]. These unique properties make them to be utilized in automotive, aerospace, oil and gas, and medical industries [4–6]. Various techniques have been employed to deposit the DLC coatings such as the Physical Vapour Deposition (PVD) [7,8], Chemical Vapour Deposition (CVD) [9,10], and electro deposition methods [11,12]. It is worth mentioning that using different techniques could result in a wide range of mechanical and electrochemical properties [13–15]. The critical factor to determine these properties of coatings is the ratio of sp^3/sp^2 bonded carbon (diamond with sp^3 hybridization and graphite with sp^2 hybridization) [16,17]. Changing the process parameters in each technique as well as the carbon source (target or gas) change the sp^3/sp^2 ratios of DLC coatings [18–20].

Moreover, the properties of DLC coatings are modified by doping various elements such as iron [21], titanium [22], nitrogen [23], silicon [7], and fluorine [24]. It has been shown that doping metallic elements changes the structure of the coating, surface roughness, and wear resistance. It has been also reported that metallic dopants result in the formation of carbides which significantly change the mechanical and electrochemical properties of the coating [25–27]. Regarding non-metallic elements, incorporation of the silicon to DLC coating decreases internal stress and improves tribological behaviour [28,29]. Furthermore, silicon-doped DLC coatings represent high corrosion resistance due to their dense coating structure which prevent chloride ions attack [30]. On the other hand, doping fluorine into DLC leads to a decrease in the number of dangling bonds which subsequently reduces surface energy of the DLC coatings [30]. Moreover, nitrogen incorporation to the DLC gives rise to the transformation of sp^3 to sp^2 carbon hybridization [31]. Accordingly, the adhesion of the nitrogen-doped DLC coating is improved due to its lower internal stress compared to the DLC coating. By doping nitrogen to the DLC coating, the band gap is reduced, which results in higher electrical conductivity of the coating [32].

The corrosion behaviour of DLC coating is influenced by the ratio of sp^3/sp^2 hybridized carbon atoms, porosity, roughness, and chemical structure of the coated layer [13,33]. On the other hand, few studies showed that the doping element affects the electrochemical behaviour and corrosion resistance of the coating [34,35]. To justify these observations, some researchers suggested that the dopant changes the passivation behaviour of the DLC coating by forming an inert oxide compound on the surface which enhances the corrosion resistance [36]. On the other hand, depending on doping element, defects of the DLC structure can be decreased or increased. Khun et al. [37] reported that the incorporation of nitrogen to the tetrahedral amorphous carbon (ta-C:N) coating, causes nitrogen aggregation which decreases corrosion resistant.

* Corresponding author.
E-mail address: mahboubi@aut.ac.ir (F. Mahboubi).

https://doi.org/10.1016/j.diamond.2019.04.007
Received 19 January 2019; Received in revised form 12 March 2019; Accepted 4 April 2019
Available online 06 April 2019
0925-9635/

Table 1
Chemical compositions of the 316 stainless steel (wt%).

Fe	Cr	Ni	Mo	Mn	Si	Cu	V	Co	C
66.5	16.9	11.7	2.5	1.52	0.49	0.50	0.08	0.07	0.02

Most of the previous researches regarding effect of doping element in DLC coating have been focused on the tribological and mechanical properties. Nonetheless, studies on their corrosion behaviour are rather scarce. To the best of our knowledge, the comprehensive study on the corrosion behaviour of DLC coatings have not been studied yet. The main aim of this study is to evaluate the influence of nitrogen doping on the corrosion behaviour of DLC coatings deposited by PACVD technique.

2. Materials and methods

The AISI 316 austenitic stainless steel was used in this study as a substrate, which its chemical composition is given in Table 1. Specimens dimension was 20 mm × 20 mm × 2 mm. Samples were grounded with 400, 600, 800 and 1200 SiC papers and polished mechanically with diamond paste. Thereafter, samples were cleaned in ultrasonic bath using acetone, and subsequently were rinsed with distilled water.

In order to achieve the adequate adhesion of the films to the substrate, the plasma nitriding was applied by the direct current (DC) pulsed plasma assisted chemical vapour deposition (PACVD) technique at 450 °C for 4 h in an atmosphere containing nitrogen (75 sccm) and hydrogen (25 sccm). Afterwards, the diamond-like carbon coating (DLC) and nitrogen doped diamond-like carbon coating (N-DLC) were deposited by the DC pulsed PACVD technique at a temperature of 120 °C for 90 min. The duty cycle, frequency, and the chamber pressure was 75%, 10 kHz, and 5 mbar, respectively. The flowrates of methane and argon were 10 sccm and 40 sccm for DLC deposition, and the flowrates of the nitrogen, methane, and argon were 10 sccm, 10 sccm, and 40 sccm, respectively for N-DLC deposition. Three samples were used for each measurement.

Raman analysis was performed to study the chemical bonding structure of the coatings by Horiba Yvon Xplora visible Raman spectroscopy. The analyses were performed over a wavelength range of 800

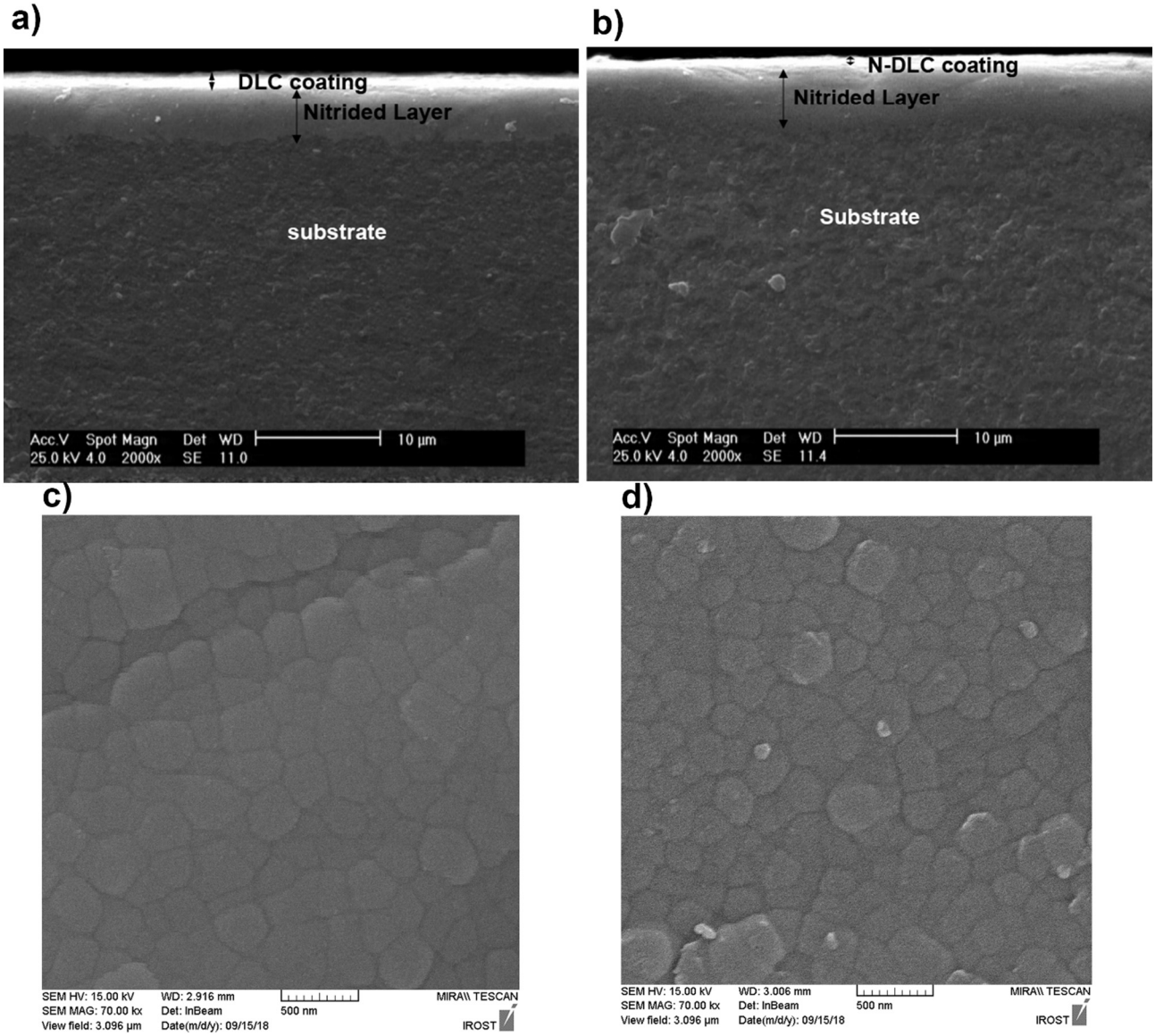

Fig. 1. The SEM cross-sectional images of a) DLC and b) N-DLC coatings. N10 T120 specimen and substrate. The FESEM surface morphology of c) DLC and d) N-DLC coatings.

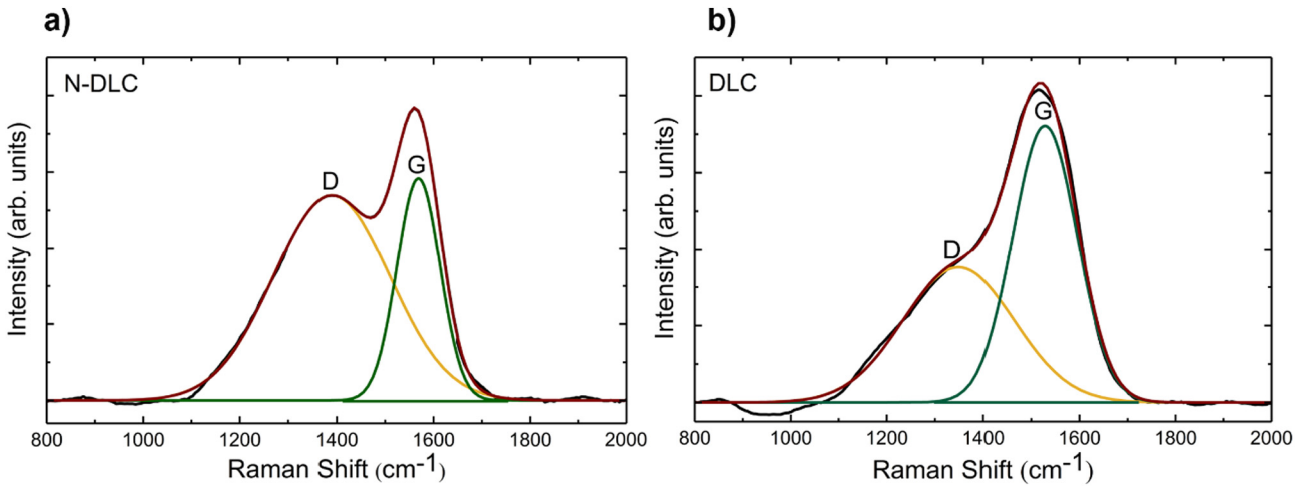

Fig. 2. The deconvlouted Raman spectra of the a) N-DLC and b) DLC coatings.

Table 2
The Raman results obtained by fitting of the spectra of the coatings.

Specimen	I_D/I_G	G position (cm^{-1})	FWHM of G (cm^{-1})
DLC	0.48 ± 0.006	1530 ± 15	157 ± 1.9
N-DLC	0.93 ± 0.008	1567 ± 14	104 ± 1.7

to 2000 cm^{-1}. In order to evaluate the Raman spectrum results, the D and G peaks were fitted to Gaussian curves.

To study the surface morphology and roughness of the coatings, the Atomic Force Microscopy (AFM) measurement were performed. Contact angle measurements were carried out by OCA 15 plus system using water and diiodomethane liquids. Moreover, the surface energies of the specimens were calculated using the Owens–Wendt model.

Potentiodynamic polarization measurements of samples were conducted in 3.5 wt% NaCl solution, at room temperature using an AUTOLAB PGSTAT 302 N instrument. A conventional three electrode setup cell was used for the measurements. The coated sample with the surface area of 1 cm^2 was assigned as a working electrode, Saturated Calomel Electrode (SCE) was served as the reference electrode, and a platinum plate was used as the auxiliary electrode. The potential scan rate of Tafel polarization tests was 1 mV/s in potential range of 0.2 V to 1 V relative to open circuit potential (OCP). Electrochemical Impedance Spectroscopy (EIS) test was applied in 3.5 wt% NaCl aqueous solution over the frequency ranging from 100 kHz to 10 mHz with a 5 mV (peak to peak) amplitude signal. All of the corrosion tests were performed three times in order to be sure about reproducibility.

The X-ray photoelectron spectroscopy (XPS) was applied on the surface of the coatings before and after immersion in 3.5 wt% NaCl solution for one week using Gammadata-scienta ESCA 200. The XPS analyses were conducted at a pressure of 10^{-9} Torr, and the power of 200 W. The atomic percentage and peak fitting of the spectra were calculated by Casa XPS software. The linear background adoption for C1s peaks and the same Full-Width Half Maximum (FWHM) for sub peaks are considered.

3. Results and discussion

3.1. Cross section and surface morphology

Fig. 1a and b illustrate the SEM cross-sectional micrographs of the DLC and N-DLC coatings. The thickness of the N-DLC and DLC coatings are 710 nm and 850 nm. By implementation of nitrogen gas inside the chamber, the deposition rate and the coating thickness decrease. Because the most important factor in the deposition of the coating is the presence of hydrocarbon components in the plasma. By introducing the nitrogen gas flow rate in the plasma, the amount of hydrocarbon components and the deposition rate are reduce. The surface morphology of DLC and N-DLC coatings are shown in Fig. 1c and d which illustrate the cauliflower-like structure of the coatings. The carbon-amorphous regions which are called nodules are bonded to each other.

3.2. Raman spectroscopy

Raman analysis is a non-destructive method to evaluate the structure of the hydrogenated DLC coating. Two main peaks of D & G in Raman spectra of the DLC coatings are located at around 1350 cm^{-1} and 1550 cm^{-1}, respectively. The G peak arises from the bond stretching of all sp^2 atom pairs and the D peak initiates from the disordering of the sp^2 atom pairs in rings [38]. Three main parameters for evaluating the structure of the DLC coatings are namely: the intensity ratio of D to G peak (I_D/I_G), position and Full width at half maximum (FWHM) of the G peak. The de-convoluted Raman spectra of the N-DLC and DLC coatings are shown in Fig. 2a and b, respectively. Three typical parameters which were mentioned above are listed in Table 2. By doping of nitrogen into the DLC coating, the I_D/I_G ratio are increased and the G peak position is shifted to the higher wavelengths, in contrast, the FWHM of the G peak is decreased. Results imply that by incorporation of nitrogen to the DLC, the structure of the coating becomes more graphitized. By nitrogen doping to the structure of the DLC coating, hydrogen replacement by nitrogen atoms decreases the amount of C—H bonds and accelerates the transformation of sp^3 to sp^2. It is due the fact that the C—H bonds in the DLC coating play a key role to stabilize the sp^3 carbon bonds [39].

3.3. AFM

Three-dimensional AFM images of the surface morphology of the DLC and N-DLC coatings are shown in Fig. 3a and b. Images show nodules on the surface of the coatings which are formed by bonding of amorphous-carbon regions. In order to determine the surface roughness, two-dimensional AFM images of the coatings surfaces are shown in Fig. 4a and b. The corresponding surface roughness profiles from black line in two-dimensional images of the N-DLC and DLC specimens are shown in Fig. 5a and b. The height difference between peaks and valleys in the N-DLC sample is greater than that of DLC specimens which demonstrates more asperities are formed on the surface of N-DLC coating. The Root Mean Square (RMS) roughness of the coatings from an area of 20 × 20 μm^2 was calculated to be 64 nm and 148 nm for DLC and N-DLC coatings, respectively. The presence of nitrogen ions in the plasma atmosphere leads to more ion bombardment and etching on the

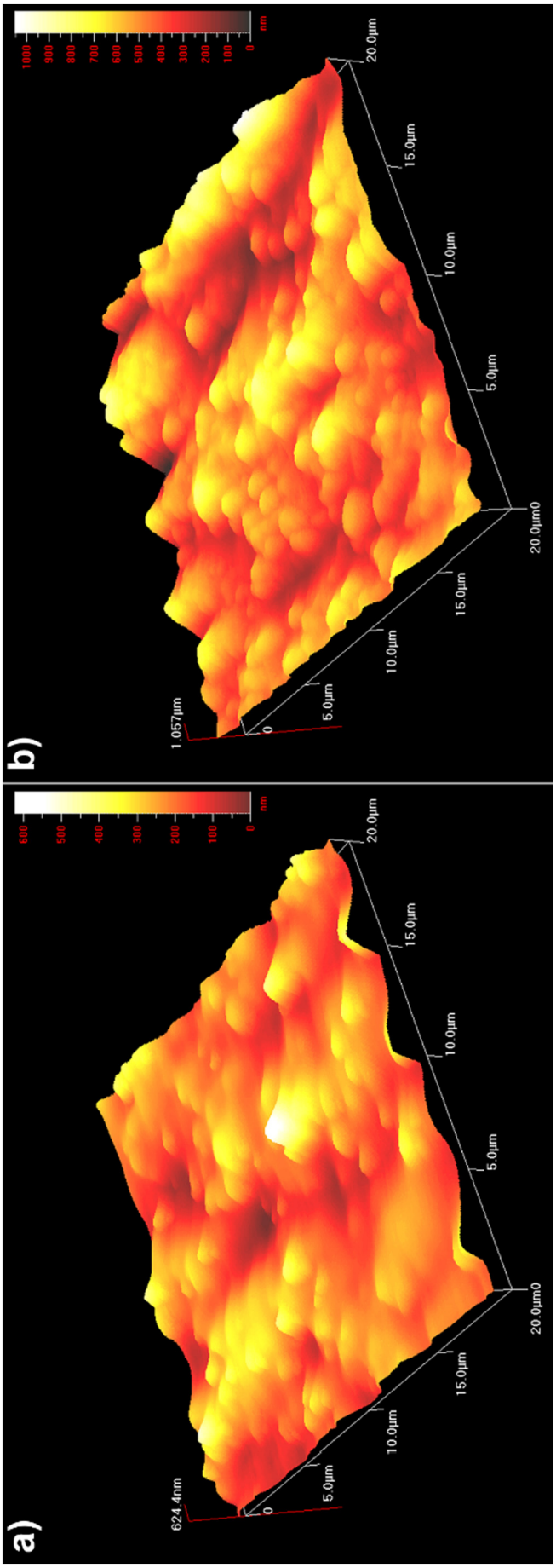

Fig. 3. 3D AFM images of the surface morphology of the a) DLC and b) N-DLC coatings.

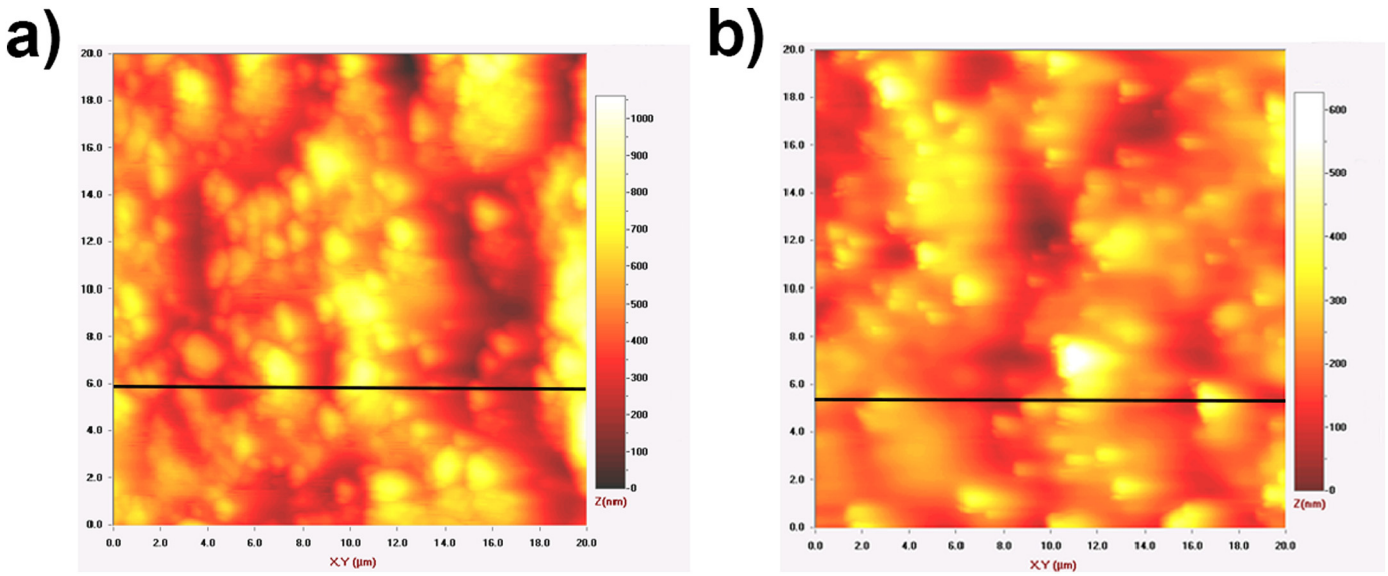

Fig. 4. 2D AFM images of the a) N-DLC and b) DLC coatings.

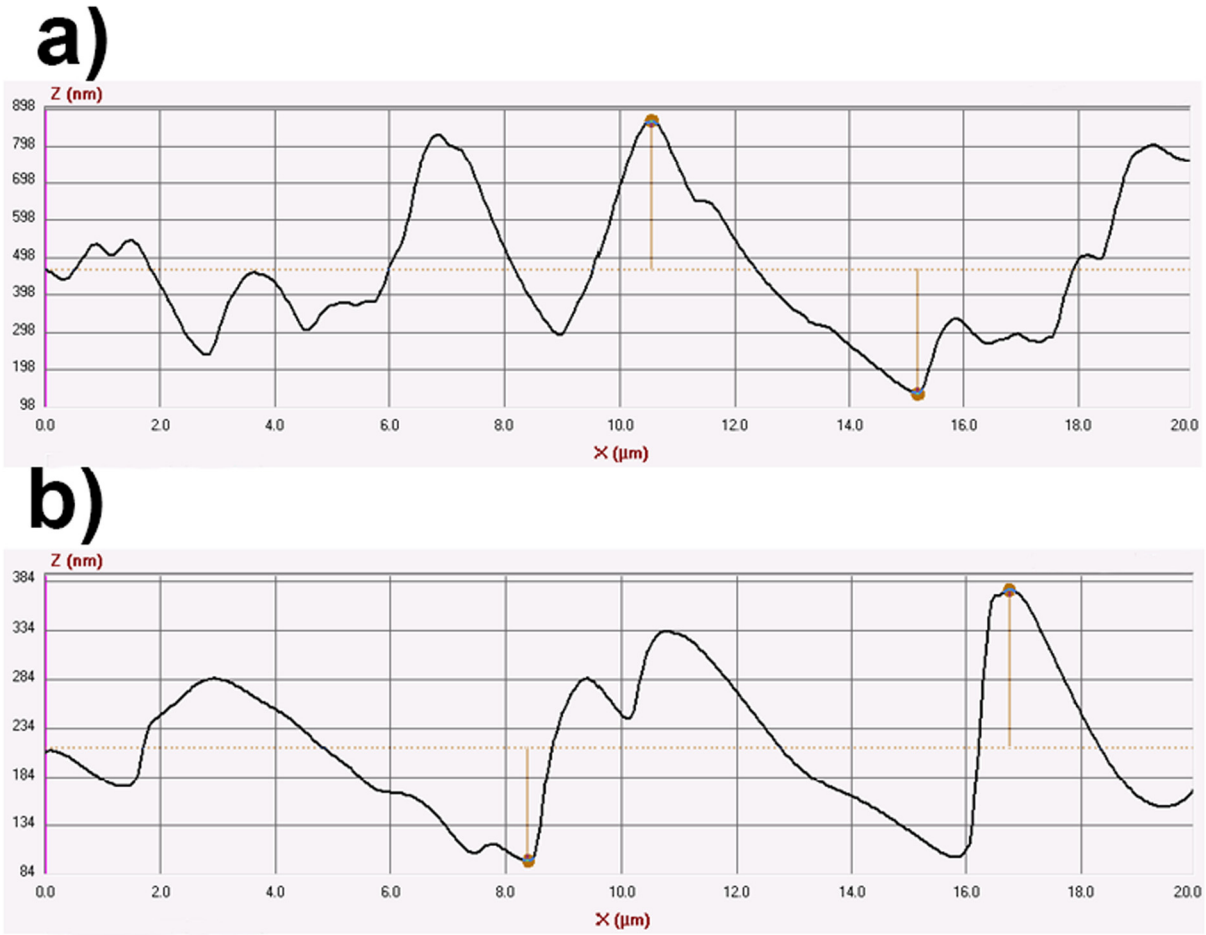

Fig. 5. Surface roughness profile of the a) N-DLC and b) DLC coatings.

N-DLC coating surface than DLC sample, and results in its higher surface roughness.

3.4. Wettability

The wettability of DLC and N-DLC coatings was studied via static contact angles measurement using water and diiodomethane liquids. The water and diiodomethane drops on the coatings surface and corresponding contact angle values are shown in Fig. 6a–d. The contact angle of the DLC and N-DLC coatings using water drop are respectively 57° and 45°. Moreover, the measured values of diiodomethane drop are 32° and 23° for DLC and N-DLC samples, respectively. The lower contact

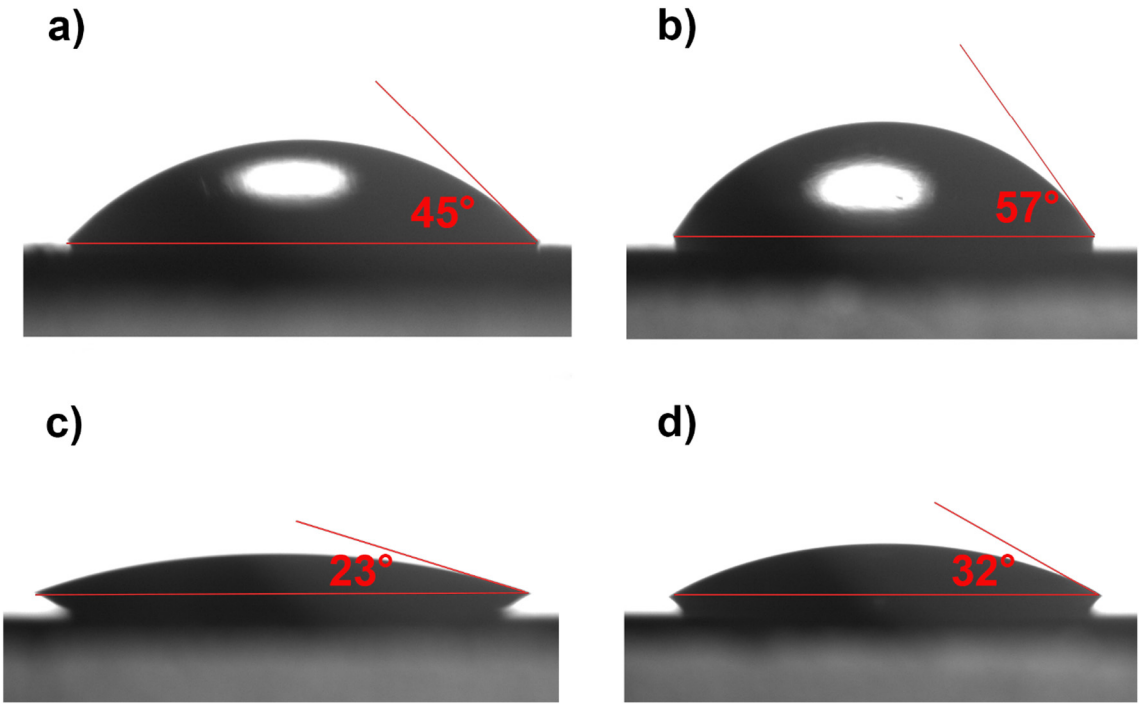

Fig. 6. Image of water drop placed on the a) N-DLC and b) DLC coatings. Image of diiodomethane drop placed on the c) N-DLC and d) DLC coatings.

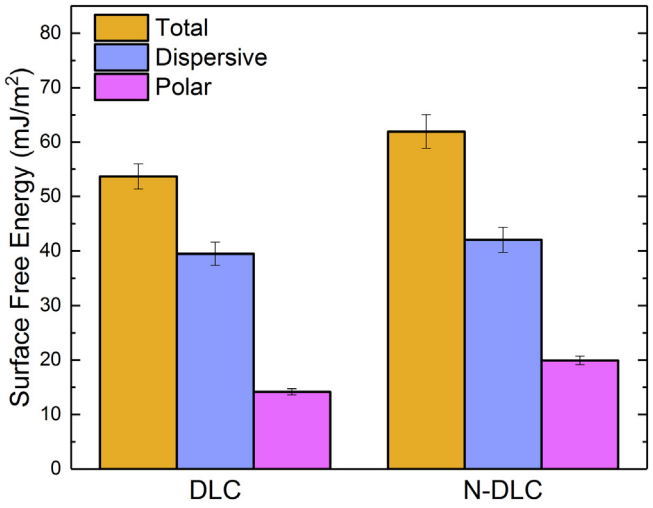

Fig. 7. The total surface energy and its corresponding dispersion and polar components of the coatings.

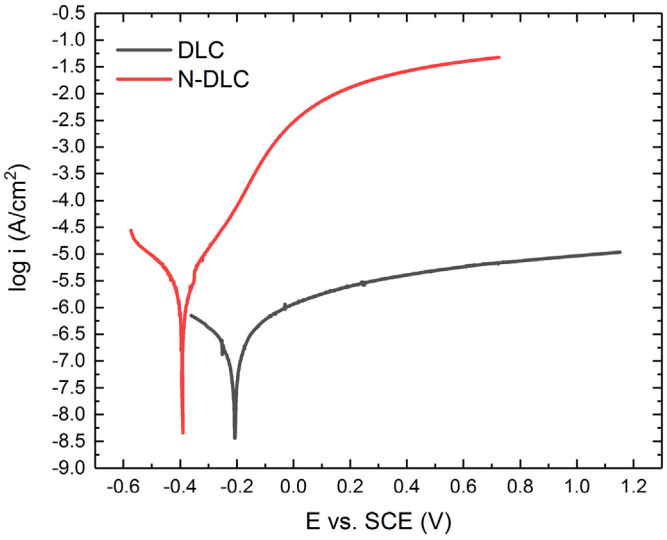

Fig. 8. Typical potentiodynamic polarization curves of the coatings immersed in 3.5 wt% NaCl solution at room temperature.

angle values of the N-DLC sample confirms its higher wettability.

In order to assess the surface energy of the coatings, the Owens–Wendt model was used in the form of following equation [34].

$$\gamma_l \bullet (1 + cos\theta) = 2\left(\sqrt{\gamma_s^d \bullet \gamma_l^d} + \sqrt{\gamma_s^p \bullet \gamma_l^p}\right) \quad (1)$$

where θ is the contact angle, γ stands for surface free energy, superscript d and p denote dispersive and polar components. The γ_l^p and γ_l^d for water are 51 mJ/m^2 and 21.8 mJ/m^2, respectively. For diiodomethane, these values are 0.38 mJ/m^2 and 50.42 mJ/m^2 [40]. Fig. 7 shows the calculated total surface energy and its corresponding dispersive and polar components of the samples. The total surface energy of the DLC specimen is 53.65 mJ/m^2 which its dispersive and polar components are 39.48 mJ/m^2 and 14.17 mJ/m^2, respectively. The total surface energy of the N-DLC sample is approximately 61.93 mJ/m^2 including the dispersive energy of 42.02 mJ/m^2 and the polar energy of 19.91 mJ/m^2. According to the obtained results, the surface energy of the N-DLC coating is higher than that of the DLC coating.

As discussed previously in Section. 3.2, the surface roughness value of the N-DLC coating is higher than the DLC coating. According to the Wenzel's theory [34], the hydrophilic surfaces (θ < 90°) become more hydrophilic with increasing surface roughness. In other words, by increasing the surface roughness of the DLC coating as a result of the nitrogen doping, its wettability increases. Moreover, by incorporation of the nitrogen atoms to the DLC coating and the replacement of the hydrogen atoms with them, the number of dangling bonds on the surface of the coating is reduced. The dangling bonds on the surface reduce the wettability of the coating due to the presence of hydrogen bonds [41]. Therefore, the N-DLC coating shows a higher wettability due to its lower dangling bonds.

Table 3
Corrosion characteristics of the coatings in 3.5 wt% NaCl solution.

Specimen	E_{corr} (mV)	i_{corr} (A/cm^2)	β_a (V/dec)	β_c (V/dec)
DLC	−206 ± 8	(6.65 ± 0.16) × 10^{-6}	0.623 ± 0.035	0.512 ± 0.032
N-DLC	−391 ± 12	(5.24 ± 0.13) × 10^{-6}	0.227 ± 0.018	0.487 ± 0.021

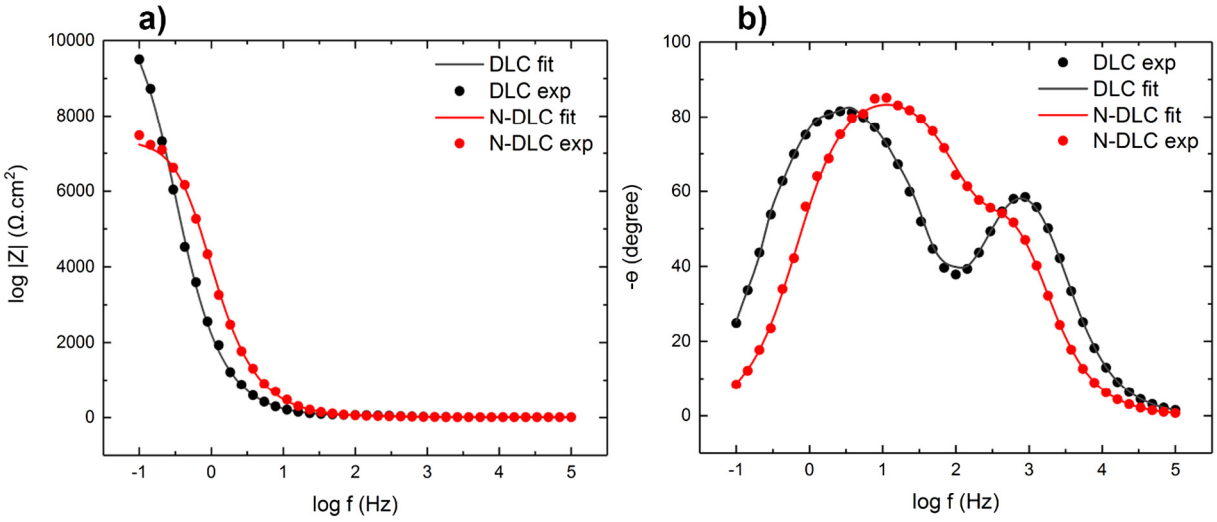

Fig. 9. Bode plots of a) |Z| vs. frequency, and b) degree vs. frequency of the coatings immersed in 3.5 wt% NaCl solution at room temperature.

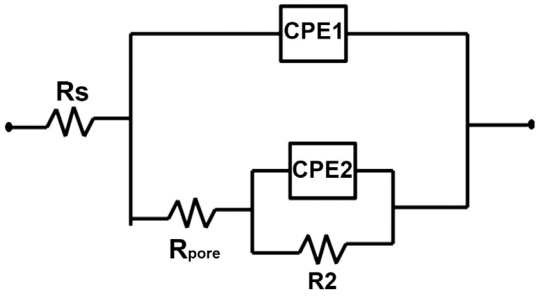

Fig. 10. Equivalent circuit model used in the fitting of the impedance data.

3.5. Potentiodynamic polarization

The corrosion behaviour of the coated samples was evaluated in a 3.5 wt% NaCl solution through polarization technique. The polarization curves of the samples are shown in Fig. 8. The values of the corrosion potential (E_{corr}), corrosion current density (i_{corr}), anodic Tafel slope (β_a) and cathodic Tafel slope (β_c) were calculated using Tafel extrapolation and summarized in Table 3. The corrosion potential of the N-DLC coating is −391 mV and that of the DLC coating is −206 mV. The corrosion current density of the DLC sample was lower than N-DLC sample which represent its better corrosion resistance.

Based on Fig. 8, DLC shows a passive region in the range of −0.17 V to 1.1 V. On the other hand, polarization curves of the N-DLC coating shows initially increase in current density from −0.3 V to −0.1 V. Thereafter, by shifting the potential to positive values, current density increases with lower rate. It should be noted that, the DLC polarization curve shows a passive region in a wider potential range which demonstrates the formation of more stable passive layer compared to the N-DLC coating. As shown in the aforementioned section, the incorporation of nitrogen atoms to the DLC coating increases its wettability. With increasing wettability, the contact area of the coating with electrolyte solution increases and intensifies the corrosion attack, which in turn accelerates the dissolution of the carbon and nitrogen atoms. On the other hand, the formation of stable passive layer on the surface of the DLC coating reduces the electrons motion rate, which subsequently decreases the corrosion current density. Nonetheless, the nitrogen aggregation in N-DLC coating causes localize corrosion [37].

3.6. Electrochemical impedance spectroscopy (EIS)

The to obtain the information of the interfacial electrochemical reactions of the coatings, EIS measurements were carried out in 3.5 wt % NaCl solution at room temperature. The Bode plots of the samples are shown in Fig. 9. As seen in the Bode plots of log |Z| vs. log f, the maximum |Z| value is obtained for DLC sample illustrating its excellent corrosion resistance (Fig. 9a). The two peaks in the plot of θ as a function of the log (f) indicate that the equivalent circuit of the samples has two time constant (Fig. 9b). Fig. 10 shows the equivalent circuit which was chosen for fitting process and extracting the results of the EIS test. In order to obtain the best fit results, constant phase element was used instead of ideal capacitance. The parameters of the equivalent circuit elements are listed in Table 4. The R_s is the solution resistance, CPE represent the charge transfer capacitance, R_{pore} represents the

Table 4
Corrosion characteristics of the coatings by EIS measurements in 3.5 wt% NaCl solution.

Specimen	R_s (Ω·cm^2)	CPE_1 ($\Omega^{-1}\,\mu s^n \cdot cm^{-2}$)	n_1	CPE_2 ($\Omega^{-1}\,\mu s^n \cdot cm^{-2}$)	n_2	R_{por} (Ω·cm^2)	R_2 (Ω·cm^2)	R_p (Ω·cm^2)
DLC	6 ± 1.1	94.7 ± 6.2	0.6921 ± 0.03	68.6 ± 5.7	0.7553 ± 0.04	70 ± 0.5	10,291 ± 99	10,361 ± 98
N-DLC	8 ± 1.4	66.3 ± 5.5	0.7955 ± 0.03	38.5 ± 2.9	0.613 ± 0.04	61 ± 0.4	7182 ± 69	7243 ± 68

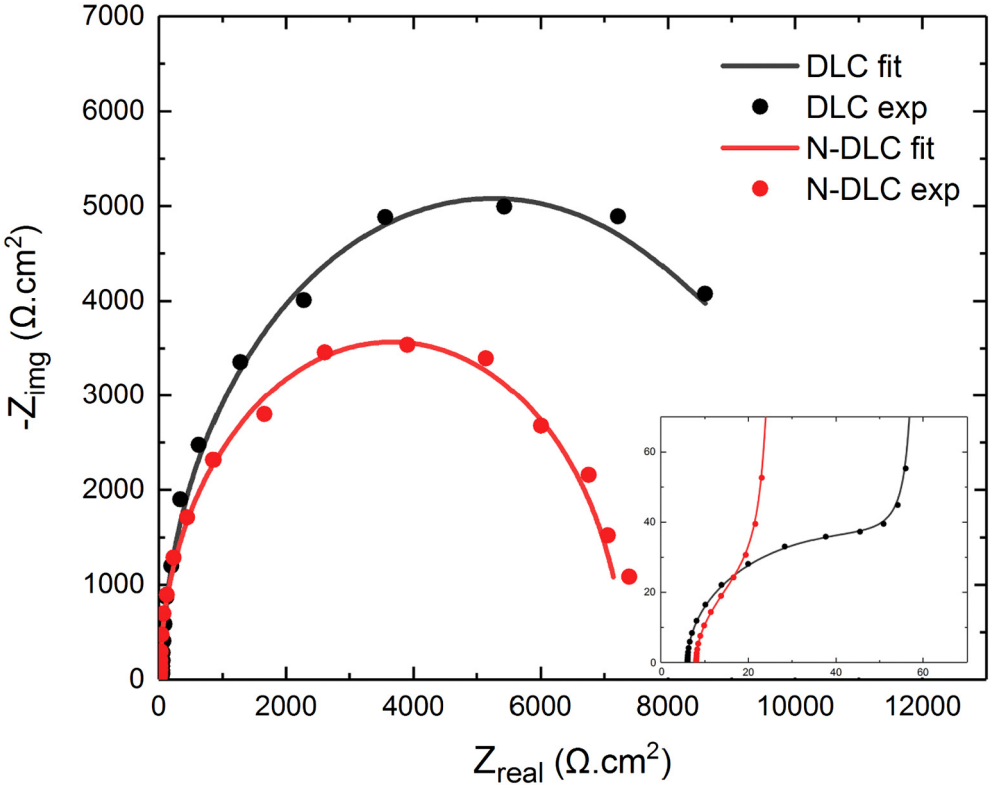

Fig. 11. Nyquist plots of the coated samples.

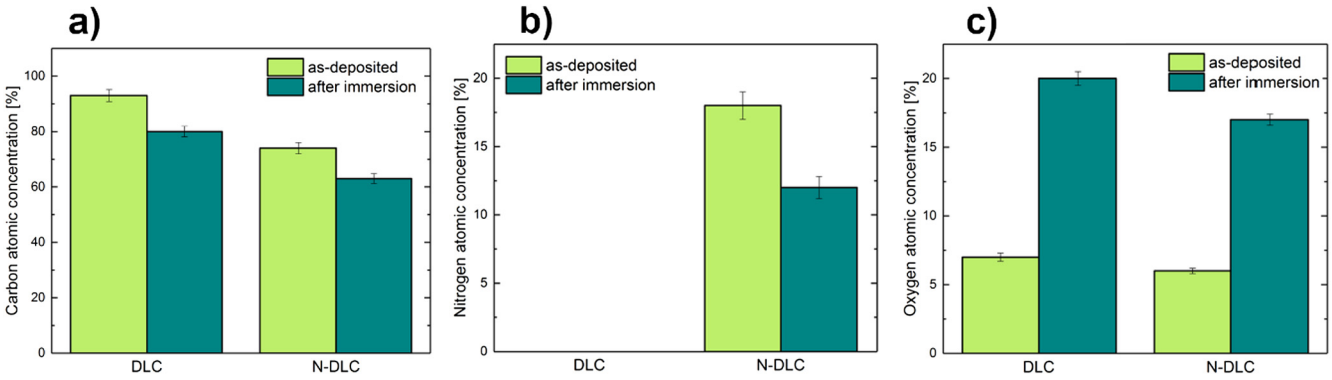

Fig. 12. Chemical composition from XPS survey spectra of the coatings before and after immersion in 3.5 wt% NaCl solution for one week.

pores resistance of the coated layer and R_p is the polarization resistance.

One of the most important parameters of the EIS test is the diameter of semi-circles. The diameter of the capacitive loop in Nyquist plots demonstrates the corrosion resistance, which in this case was higher in the DLC sample compared to the N-DLC sample (Fig. 11). The polarization resistance of the DLC and the N-DLC sample was 10,361 Ω·cm^2 and 7243 Ω·cm^2. Additionally, the CPE value of the DLC and N-DLC samples was 68.6 μS·cm^{-2} and 38.5 μS·cm^{-2}. The higher values of the constant phase element of the N-DLC coating are associated to its higher surface roughness, which increases the accumulation of corrosive ions at the interface of electrolyte and coating. According to the Raman results obtained in Section 3.2, by doping of nitrogen atoms, the structure of the coating becomes more graphitized. In the graphite structure, there are free electrons between the graphite plates. By decreasing the sp^3/sp^2 ratio in the N-DLC coating, free electrons in the structure are increased and corrosion rate rises. Furthermore, with incorporation of the nitrogen atoms in the DLC structure, nitrogenous compounds such as pyridine, pyrrole, and nitrile are formed which have non-bonded electrons [42]. The presence of these electrons in the structure increases the electrical conductivity and the electron consumption at the coating surface.

3.7. X-ray photoelectron spectroscopy

The variations of carbon, nitrogen and oxygen atomic concentrations of the coatings using XPS analysis before and after being immersed in 3.5 wt% NaCl solution for one week are shown in Fig. 12. The carbon content of the DLC coating before and after immersion is obtained to be 92% and 80%. For N-DLC specimen, it is also observed that carbon concentration dropped from 74% to 63% after corrosion test. Reduction of carbon percentage in both coatings represents the dissolution of carbon atoms during the corrosion test. In addition, after immersing the N-DLC sample in the corrosive solution, the nitrogen content drops from 18% to 12%, indicating the dissolution of nitrogen atoms. On the other hand, the oxygen percentage of the DLC sample increased from 5% to 20% and for the N-DLC sample, it is rose from 6% to 17% after immersion.

The C1s high-resolution peaks of DLC and N-DLC coatings before

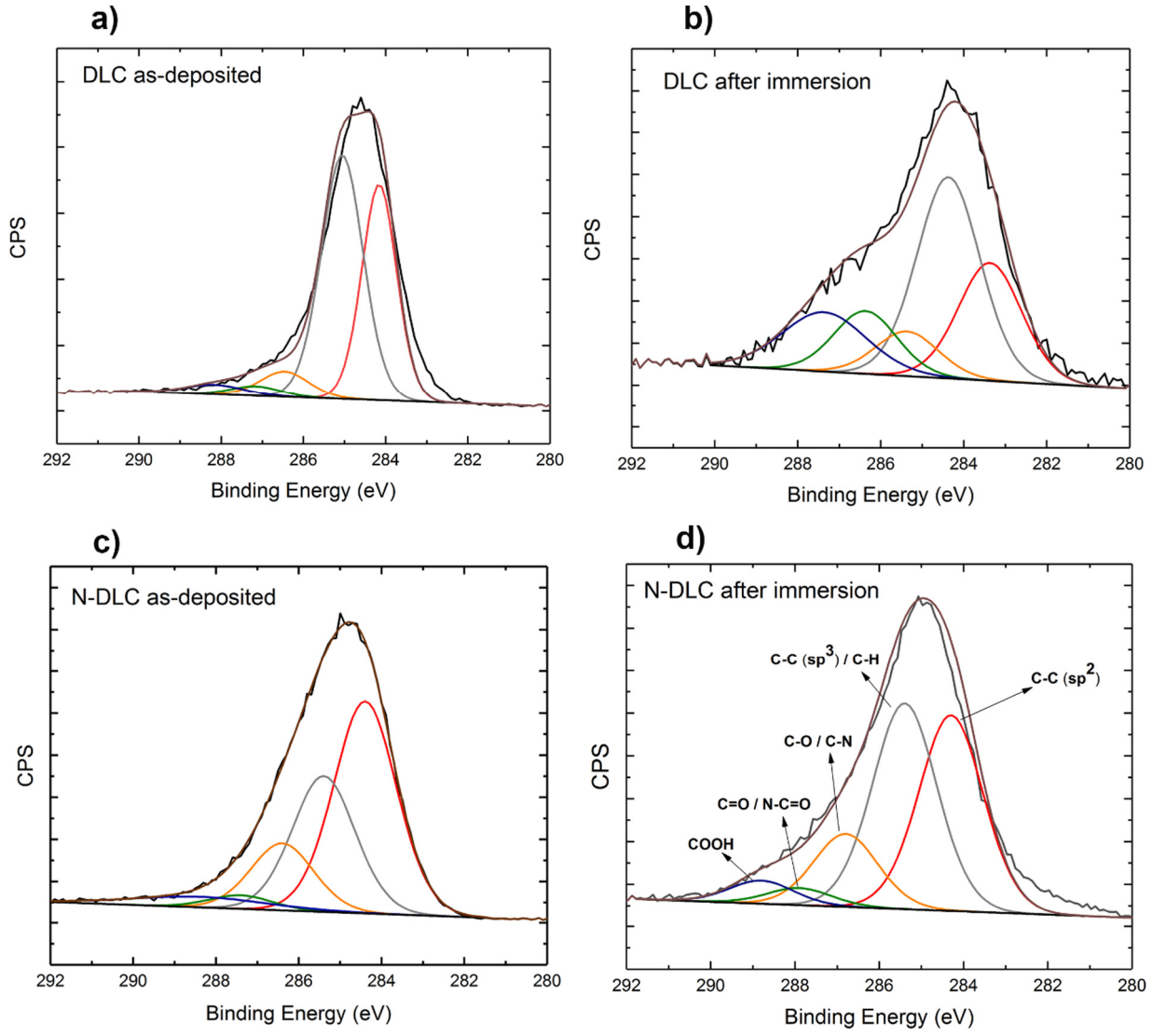

Fig. 13. The C1s high-resolution peaks of the DLC coating a) as-deposited and b) after immersion in the 3.5 wt% NaCl solution. The C1s high-resolution peaks of the N-DLC coating c) as-deposited and d) after immersion in the 3.5 wt% NaCl solution.

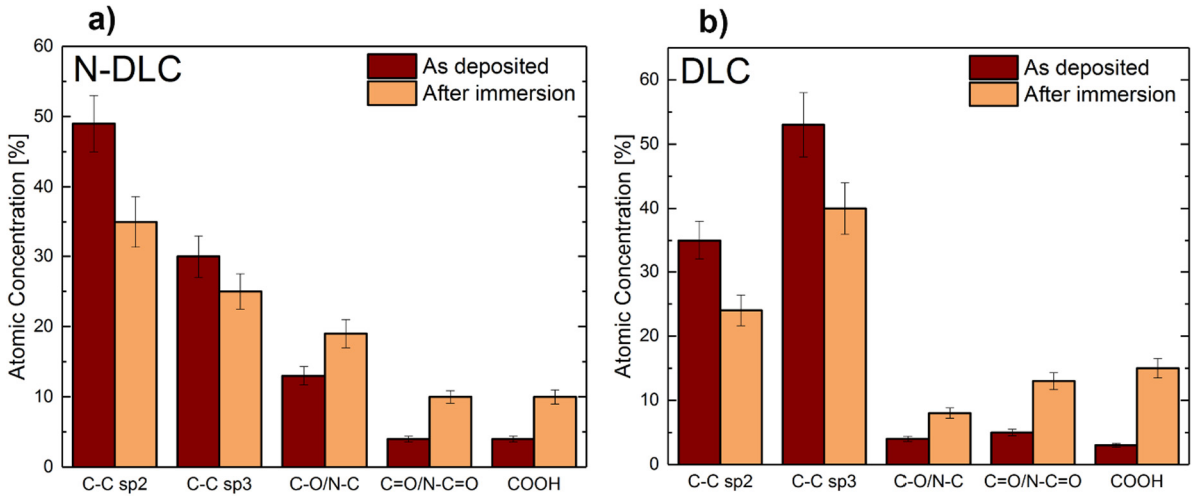

Fig. 14. Atomic concentrations of peak deconvoluted C1s components of the a) N-DLC, and b) DLC coatings before and after immersion in the 3.5 wt% NaCl solution.

and after immersion in the 3.5 wt% NaCl solution are shown in Fig. 13a–d. The C1s peak was de-convoluted into five sub-peaks corresponding to the different bonding state of C atoms. This peak consists of C_1: C−C (sp^2) at binding energy (BE) of about 284.1 eV, C_2: C−C (sp^3)/C−H at BE ≃ 285.3 eV, C_3: C−O/C−N at BE ≃ 286.5 eV, C_4:C═O/N−C═O at BE ≃ 287.5 eV, and C_5: COOH at BE ≃ 289 eV [43–45]. As shown in Fig. 11, with doping of the nitrogen atoms to the DLC structure, the C1s peak becomes broader due to their bonds with carbon atoms. However, after the samples were immersed in corrosive medium, oxide and carboxylic compounds were observed in de-convoluted C1s peaks.

Fig. 14a confirms the more pronounced presence of C−C (sp^2) bonds in nitrogen-doped DLC coating (as-deposited). Moreover, evaluation of the oxygen concentration in both as-deposited coatings shows that the concentration of the oxide (C−O and C═O) and carboxylic (COOH) bonds are almost the same for the both coatings (Fig. 14a and b). However, the higher C−O/N−C bonds content in as-deposited N-DLC in comparison to as-deposited DLC is related to the presence of N−C bonds. On the other hand, after the immersion test, it is observed that in both coatings, the C−C (sp^2) and C−C (sp^3) carbon bonds decrease, whereas the sp^2 carbon bonds decrease is more noticeable. The amount of oxide and carboxylic compounds increases in both coatings and in this case DLC sample shows more increase of C═O and COOH bonds compared to N-DLC sample.

The higher reduction of C−C (sp^2) bonds compared to C−C (sp^3) bonds could be attributed to the weak Van der Waals bonds between the graphite plates. The penetration of the chloride ions between the graphite plates causes the graphite exfoliation and dissolution of the carbon atoms bonded in sp^2 hybridization. Considering the higher content of the C−C (sp^3) bonds and the higher concentration of the oxide and carboxylic bonds in the DLC sample, it can be concluded that the corrosion resistant improvement of the DLC specimen is as a result of the sp^3 carbon bonds which facilitate formation of the passive layer. The high corrosion rate of the N-DLC coating obtained in Sections 3.4 and 3.5, as well as the observation of lower oxide and carboxylic compounds (C═O and COOH) in the XPS test, demonstrate that the passive layer was unstable in this specimen.

4. Conclusion

The effect of nitrogen doping on the corrosion behaviour of DLC coating was investigated through structural evolution and electrochemical measurements. Raman spectroscopy results showed that by incorporation of the nitrogen to the DLC coating, its structure becomes more graphitized. Moreover, AFM and contact angle studies showed that nitrogen-doped DLC coating had a higher surface roughness and surface energy compared to the DLC coating. Corrosion studies on samples showed that the corrosion density for the N-DLC and DLC samples was 5.24×10^{-6} A/cm^2 and 6.65×10^{-6} A/cm^2, respectively. Additionally, EIS test results showed that the DLC coating has better corrosion resistance than the nitrogen-doped DLC coating. The polarization resistance of the DLC and the N-DLC sample was 10,361 Ω·cm^2 and 7243 Ω·cm^2. By comparing the XPS results of the samples before and after immersion, it was found that the sp^2 carbon bonds decreased more than sp^3 carbon bonds and the amount of C═O and COOH bonds in DLC sample increased more compared to N-DLC sample. The XPS investigation of the DLC and N-DLC coatings reveals that the presence of sp^3 carbon bonds play a key role in formation of the passive layer.

References

[1] A. Hatem, J. Lin, R. Wei, R.D. Torres, C. Laurindo, P. Soares, Surface & Coatings Technology Tribocorrosion behavior of DLC-coated Ti-6Al-4V alloy deposited by PIID and PEMS + PIID techniques for biomedical applications, Surf. Coat. Technol. (2017), https://doi.org/10.1016/j.surfcoat.2017.07.004.

[2] W. Behaviors, T. Dlc, Author's accepted manuscript, Ceram. Int. (2017), https://doi.org/10.1016/j.ceramint.2017.12.074.

[3] J. Solis, H. Zhao, C. Wang, J.A. Verduzco, A.S. Bueno, A. Neville, Applied surface science tribological performance of an H-DLC coating prepared by PECVD, Appl. Surf. Sci. 383 (2016) 222–232, https://doi.org/10.1016/j.apsusc.2016.04.184.

[4] S. Thirumalai, A. Hausberger, J.M. Lackner, W. Waldhauser, T. Schwarz, Surface & coatings technology effect of the type of elastomeric substrate on the microstructural, surface and tribological characteristics of diamond-like carbon (DLC) coatings, Surf. Coat. Technol. 302 (2016) 244–254, https://doi.org/10.1016/j.surfcoat.2016.06.021.

[5] A. Choleridis, S. Sao-joao, J. Ben-mohamed, D. Chern, V. Barnier, G. Kermouche, C. Heau, M. Leroy, J. Fontaine, S. Descartes, Surface & coatings technology experimental study of wear-induced delamination for DLC coated automotive components, Surf. Coat. Technol. 352 (2018) 549–560, https://doi.org/10.1016/j.surfcoat.2018.08.048.

[6] Y. Ju, T. Fei, M. Jun, K. Ho, Applied surface science synthesis and electrochemical properties of Ti-doped DLC films by a hybrid PVD/PECVD process, Appl. Surf. Sci. 433 (2018) 1184–1191, https://doi.org/10.1016/j.apsusc.2017.10.151.

[7] D. Bociaga, A. Sobczyk-Guzenda, W. Szymanski, A. Jedrzejczak, A. Jastrzebska, A. Olejnik, L. Swiatek, K. Jastrzebski, Diamond like carbon coatings doped by Si fabricated by a multi-target DC-RF magnetron sputtering method - mechanical properties, chemical analysis and biological evaluation, Vacuum 143 (2017) 395–406, https://doi.org/10.1016/j.vacuum.2017.06.027.

[8] D. Bootkul, B. Supsermpol, N. Saenphinit, C. Aramwit, S. Intarasiri, Nitrogen doping for adhesion improvement of DLC film deposited on Si substrate by Filtered Cathodic Vacuum Arc (FCVA) technique, Appl. Surf. Sci. 310 (2014) 284–292, https://doi.org/10.1016/j.apsusc.2014.03.059.

[9] L. Kolodziejczyk, W. Szymanski, D. Batory, A. Jedrzejczak, Nanotribology of silver and silicon doped carbon coatings, Diam. Relat. Mater. 67 (2016) 8–15, https://doi.org/10.1016/j.diamond.2015.12.010.

[10] D. Batory, J. Gorzedowski, B. Rajchel, W. Szymanski, L. Kolodziejczyk, Silver implanted diamond-like carbon coatings, Vacuum 110 (2014) 78–86, https://doi.org/10.1016/j.vacuum.2014.09.001.

[11] R. Paul, S. Dalui, S.N. Das, R. Bhar, A.K. Pal, Applied surface science hydrophobicity in DLC films prepared by electrodeposition technique, 255 (2008) 1705–1711, https://doi.org/10.1016/j.apsusc.2008.06.015.

[12] T.M. Manhabosco, I.L. Muller, Electrodeposition of diamond-like carbon (DLC) films on Ti, Appl. Surf. Sci. 255 (2009) 4082–4086, https://doi.org/10.1016/j.apsusc.2008.10.087.

[13] E.L. Dalibón, L. Escalada, S. Simison, C. Forsich, D. Heim, S.P. Brühl, Mechanical and corrosion behavior of thick and soft DLC coatings, Surf. Coat. Technol. 312 (2017) 101–109, https://doi.org/10.1016/j.surfcoat.2016.10.006.

[14] H. Cicek, Wear behaviors of TiN/TiCN/DLC composite coatings in different environments, Ceram. Int. 44 (2018) 4853–4858, https://doi.org/10.1016/j.ceramint.2017.12.074.

[15] H. Kovac, A. Fatih, Ö. Baran, A. Çelik, Tribological behavior of DLC films and duplex ceramic coatings under different sliding conditions, 44 (2018) 7151–7158, https://doi.org/10.1016/j.ceramint.2018.01.158.

[16] M. Kabátová, M. Klich, J. Dobrovodský, The Comparison of Structure and Properties in DC Magnetron Sputtered and HiPIMS W-C: H Coatings With Different Hydrogen Content, (2018), https://doi.org/10.1016/j.ceramint.2018.09.219.

[17] C. Chou, J. Lin, R. Wu, Microstructures and mechanical properties of an a-C: N film as the interlayer and the outmost layer of a DLC-deposited Ti bio-alloy, Ceram. Int. 43 (2017) S776–S783, https://doi.org/10.1016/j.ceramint.2017.05.196.

[18] M. Ebrahimi, F. Mahboubi, M.R. Naimi-jamal, Diamond & Related Materials Wear behavior of DLC film on plasma nitrocarburized AISI 4140 steel by pulsed DC PACVD: effect of nitrocarburizing temperature, Diam. Relat. Mater. 52 (2015) 32–37, https://doi.org/10.1016/j.diamond.2014.12.004.

[19] M. Jokari-sheshdeh, F. Mahboubi, K. Dehghani, Diamond & Related Materials Structure and tribological behavior of diamond-like carbon coatings deposited on the martensitic stainless steel: the influence of gas composition and temperature, Diam. Relat. Mater. 81 (2018) 77–88, https://doi.org/10.1016/j.diamond.2017.11.007.

[20] E.L. Dalibón, D. Heim, C. Forsich, A. Rosenkranz, M.A. Guitar, S.P. Brühl, Diamond & Related Materials Characterization of thick and soft DLC coatings deposited on plasma nitrided austenitic stainless steel, Diam. Relat. Mater. 59 (2015) 73–79, https://doi.org/10.1016/j.diamond.2015.09.010.

[21] S.C. Ray, W.F. Pong, P. Papakonstantinou, Iron, nitrogen and silicon doped diamond like carbon (DLC) thin films: a comparative study, Thin Solid Films 610 (2016) 42–47, https://doi.org/10.1016/j.tsf.2016.04.048.

[22] L. Huang, J. Yuan, C. Li, D. Hong, Surface & Coatings Technology Microstructure, tribological and cutting performance of Ti-DLC/α-C: H multilayer fi lm on cemented carbide, Surf. Coat. Technol. 353 (2018) 163–170, https://doi.org/10.1016/j.surfcoat.2018.08.076.

[23] J. Corona-Gomez, S. Shiri, M. Mohammadtaheri, Q. Yang, Adhesion enhancement of DLC on CoCrMo alloy by diamond and nitrogen incorporation for wear resistant applications, Surf. Coat. Technol. 332 (2017) 120–127, https://doi.org/10.1016/j.surfcoat.2017.10.050.

[24] T. Imai, T. Harigai, T. Tanimoto, R. Isono, Y. Iijima, Y. Suda, Hydrogen-free fluorinated DLC films with high hardness prepared by using T-shape filtered arc deposition system, Vacuum. (2018) 0–1, https://doi.org/10.1016/j.vacuum.2018.07.009.

[25] A. Pardo, C. Gómez-aleixandre, Metal incorporation strategies in DLC (fullerene-like) thin films grown by ECR-CVD, Vaccum 85 (2011) 1140–1143, https://doi.org/10.1016/j.vacuum.2011.03.001.

[26] S. Gayathri, N. Kumar, R. Krishnan, T.R. Ravindran, S. Amirthapandian, S. Dash, In fluence of transition metal doping on the tribological properties of pulsed laser deposited DLC films, Ceram. Int. 41 (2015) 1797–1805, https://doi.org/10.1016/j.

ceramint.2014.09.125.
[27] S.C. Ray, W.F. Pong, P. Papakonstantinou, Iron, nitrogen and silicon doped diamond like carbon (DLC) thin films: a comparative study, Thin Solid Films 610 (2016) 42–47, https://doi.org/10.1016/j.tsf.2016.04.048.
[28] I. Tanaka, T. Nakano, H. Kousaka, H. Hashitomi, Tribological behavior of unlubricated sliding between a steel ball and Si-DLC deposited by ultra-high-speed coating employing an MVP method, Surf. Coatings Technol. 332 (2017) 128–134, https://doi.org/10.1016/j.surfcoat.2017.07.077.
[29] D. Hofmann, S. Kunkel, K. Bewilogua, R. Wittorf, Surface & coatings technology from DLC to Si-DLC based layer systems with optimized properties for tribological applications, Surf. Coat. Technol. 215 (2013) 357–363, https://doi.org/10.1016/j.surfcoat.2012.06.094.
[30] P. Papakonstantinou, J.F. Zhao, P. Lemoine, E.T. Mcadams, J.A. Mclaughlin, The Effects of Si Incorporation on the Electrochemical and Nanomechanical Properties of DLC Thin Films, vol. 11, (2002), pp. 1074–1080.
[31] C. Zeng, Q. Chen, M. Xu, S. Deng, Y. Luo, T. Wu, Diamond & Related Materials Enhancement of mechanical, tribological and morphological properties of nitrogenated diamond-like carbon films by gradient nitrogen doping, Diam. Relat. Mater. 76 (2017) 132–140, https://doi.org/10.1016/j.diamond.2017.05.004.
[32] K. Zhou, P. Ke, X. Li, Y. Zou, A. Wang, Applied surface science microstructure and electrochemical properties of nitrogen-doped DLC films deposited by PECVD technique, Appl. Surf. Sci. 329 (2015) 281–286, https://doi.org/10.1016/j.apsusc.2014.12.162.
[33] T.F. Zhang, Q.Y. Deng, B. Liu, B.J. Wu, F.J. Jing, Y.X. Leng, N. Huang, Wear and corrosion properties of diamond like carbon (DLC) coating on stainless steel, CoCrMo and Ti6Al4V substrates, Surf. Coat. Technol. 273 (2015) 12–19, https://doi.org/10.1016/j.surfcoat.2015.03.031.
[34] A. Mazare, A. Anghel, C. Surdu-bob, G. Totea, I. Demetrescu, D. Ionita, Silver doped diamond-like carbon antibacterial and corrosion resistance coatings on titanium, Thin Solid Films 657 (2018) 16–23, https://doi.org/10.1016/j.tsf.2018.04.036.
[35] W. Yang, D. Xu, Y. Gao, L. Hu, P. Ke, J. Chen, Diamond & related materials microstructure, adhesion, in vitro corrosion resistance and tribological behavior of (Si:N) -DLC coated pure Ti, Diam. Relat. Mater. 92 (2019) 109–116, https://doi.org/10.1016/j.diamond.2018.12.027.
[36] G. Irmer, E. Muller, Electrochemical corrosion behaviour of uncoated and DLC coated medical grade Co28Cr6Mo, 178 (2004) 830–837, https://doi.org/10.1016/j.surfcoat.2003.06.015.
[37] N.W. Khun, E. Liu, X.T. Zeng, Corrosion behavior of nitrogen doped diamond-like carbon thin films in NaCl solutions, Corros. Sci. 51 (2009) 2158–2164, https://doi.org/10.1016/j.corsci.2009.05.050.
[38] A.C. Ferrari, J. Robertson, Interpretation of Raman Spectra of Disordered and Amorphous Carbon, vol. 61, (2000), pp. 95–107.
[39] J. Robertson, Requirements of ultrathin carbon coatings for magnetic storage technology, Tribol. Int. 36 (2003) 405–415, https://doi.org/10.1016/S0301-679X(02)00216-5.
[40] T. Ma, Wetting behaviour of plasma sprayed oxide coatings, 252 (2006) 8514–8520, https://doi.org/10.1016/j.apsusc.2005.11.065.
[41] L. Ostrovskaya, V. Perevertailo, V. Ralchenko, A. Dementjev, O. Loginova, Wettability and surface energy of oxidized and hydrogen plasma-treated diamond films, 11 (2002) 845–850.
[42] Y. Gongyang, C. Qu, S. Zhang, M. Ma, Eliminating delamination of graphite sliding on diamond-like carbon, Carbon N.Y. 132 (2018) 444–450, https://doi.org/10.1016/j.carbon.2018.02.080.
[43] Y.S. Zou, Q.M. Wang, H. Du, G.H. Song, J.Q. Xiao, J. Gong, C. Sun, L.S. Wen, Structural characterization of nitrogen doped diamond-like carbon films deposited by arc ion plating, 241 (2005) 295–302, https://doi.org/10.1016/j.apsusc.2004.07.043.
[44] Y. Hayashi, T. Kamio, T. Soga, K. Kaneko, T. Jimbo, Efficient nitrogen incorporation into amorphous carbon films by double beam method, Diam. Relat. Mater. 14 (2005) 970–974, https://doi.org/10.1016/j.diamond.2005.01.003.
[45] J. Hao, W. Liu, Q. Xue, Effect of N 2/CH 4 flow ratio on microstructure and composition of hydrogenated carbon nitride films prepared by a dual DC-RF plasma system, 353 (2007) 136–142, https://doi.org/10.1016/j.jnoncrysol.2006.10.008.